

## Mechanisms of enhanced hexavalent chromium removal from water by bentonite stabilized zerovalent iron nanoparticles

Jiankun Zhang\*, Xueyang Zhang, Jiaqiang Liu, Linjun Zhang, Hong Zheng

School of Environmental Engineering, Xuzhou University of Technology, Xuzhou 221111, China,  
emails: zhangjiankun@xzit.edu.cn (J.K. Zhang), 343997913@qq.com (X.Y. Zhang), 67727278@qq.com (J.Q. Liu),  
wole2009@yeah.net (L.J. Zhang), 45876288@qq.com (H. Zheng)

Received 21 September 2021; Accepted 16 April 2022

---

### ABSTRACT

Using natural bentonite as carrier, bentonite-supported nano zerovalent iron (B-nZVI) was prepared by liquid phase reduction method. The composite was characterized by X-ray diffraction, scanning electron microscopy, X-ray photoelectron spectroscopy, and the effect of Cr(VI) removal by B-nZVI was investigated. The results show that the agglomeration effect of nano zerovalent iron is reduced by bentonite loading, and the composite has the structural characteristics of two materials, which can effectively remove Cr(VI) from water. The removal rate of Cr(VI) increased with the decrease of pH and Cr(VI) initial concentration, and increased with the increase of B-nZVI composite dosage and reaction time. The removal rate of Cr(VI) by B-nZVI composite accorded with pseudo-second-order reaction kinetic model.

*Keywords:* Bentonite; Nanoscale zerovalent iron; Cr; Adsorption

---

### 1. Introduction

Heavy metal pollutants are highly toxic and difficult to degrade. And have grown up to be the most serious environmental problems threatening human development [1–3]. Chromium pollution widely comes from leather, metallurgy, electroplating and other industries [4,5]. Chromium in natural environment mainly exists in two stable states: trivalent chromium (Cr(III)) and hexavalent chromium (Cr(VI)). Cr(VI) has higher solubility and strong migration, which is more harmful [6]. Cr(VI) is recognized as one of the top 16 toxic pollutants because of its teratogenic and carcinogenic properties [7]. When it enters the human body through the skin, digestive system and respiratory system, it may trigger dermatitis, rhinitis and even cancer [8]. The toxicity, carcinogenicity and mobility of hexavalent chromium (Cr(VI)) are much higher than those of trivalent chromium (Cr(III)), so it is listed as the first category of pollutants [9–11]. So how to control chromium pollution

effectively has attracted more and more attention. For more effective remediation technology of Cr(VI) contaminated in the water, various technologies have been developed including microbial-assisted phytoremediation, chemical reduction, nanomaterials applications, physical adsorption and membrane filtration [12]. Nano zerovalent iron (nZVI) has strong reducibility and is widely used for the removal of heavy metals and refractory organic matter [13–15]. The widespread applications of nZVI are attributed to its high specific surface area, large reduction capacity, high efficiency, and cost-effective nature [16]. Application of nZVI in permeable reactive barriers is promising in the field of the remediation of Cr(VI) contaminated groundwater by converting it to the less harmful Cr(III) or its precipitates [17]. However, nZVI is easy to oxidize and agglomerate, reducing the reaction efficiency and limiting its application. Supporting nZVI on a carrier can improve its dispersibility and reduce agglomeration [18,19]. Natural bentonite has a low price, large yield, large specific surface area,

---

\* Corresponding author.

special layered structure, and good adsorption and catalytic properties [20,21]. Therefore, the main purpose of this study is equivalent to investigating the structure and morphology of the prepared bentonite-supported nanometer zerovalent iron composite and using it to remove Cr(VI) in water. The effects of pH, temperature, initial concentration, dosage coexisting ions, and other factors on the removal efficiency were investigated.

## 2. Materials and methods

### 2.1. Reagents and instruments

#### 2.2.1. Reagents

Ferrous sulfate heptahydrate ( $\text{FeSO}_4 \cdot 7\text{H}_2\text{O}$ ), potassium borohydride ( $\text{KBH}_4$ ), sodium hydroxide ( $\text{NaOH}$ ), anhydrous ethanol, polyethylene glycol, bentonite were all analytically pure, and the experimental water was deionized water.

#### 2.2.2. Instruments

Fourier-transform infrared spectrometer (IS10), scanning electron microscope (SU8020), X-ray powder diffraction (X'Pert PRO MPD), X-ray photoelectron spectroscopy (ESCALAB 250Xi), UV-visible spectrophotometer (UV-2100), constant temperature vacuum drying oven (DZF-6020), gas bath constant temperature shock vibrator (ZD-85), automatic nitrogen generator (SPN-500), electric stirrer (JJ1A).

### 2.2. Preparation of materials

Weigh 2 g of the sifted bentonite and dissolve it in 100 mL deionized water. 9.9286 g of ferrous sulfate was dissolved in the bentonite system and stirred for another 24 h. After the stirring, it was transferred to the three-necked flask and aerated for 5 min under nitrogen protection. Then 40 mL anaerobic ethanol was added to the three-necked flask, stir vigorously with a precision booster electric stirrer, and add 100 mL  $\text{KBH}_4$  drop by drop to the three-neck flask. Black precipitation appeared immediately when  $\text{KBH}_4$  was added to the system. After the dripping, continue stirring for 30 min to ensure that the reaction can be completely carried out. The black residue was washed with deoxidized ethanol and deoxidized water several times,

and the waste liquid was siphoned out and dried in a vacuum drying oven for 24 h to obtain bentonite-supported nano-iron particles, which were placed in an oxygen-free brown reagent bottle for standby.

### 2.3. Characterization of materials

The surface morphology of bentonite-supported nano zerovalent iron (B-nZVI) was analyzed by scanning electron microscopy (SU8020, Hitachi, Japan). Test method of scanning electron microscope: the sample to be tested with ion sputtering coating machine spray gold, test acceleration voltage 30 kV. The surface crystal pattern of B-nZVI was analyzed by X-ray diffraction (X'Pert PRO MPD, Panaco, Netherlands). Test conditions: tube pressure 40 kV, scanning step  $0.02^\circ$ . Fourier-transform infrared spectrometer (Nicolet IS10, Thermo Fisher Scientific) was used to analyze B-nZVI surface functional groups. Test method: grind the sample to be tested and KBr powder according to mass ratio, grind evenly and press the tablet, and scan the range of  $350\text{--}4,000\text{ cm}^{-1}$ ; X-ray photoelectron spectroscopy (ESCALAB 250Xi, Thermo Fisher Scientific) was used to analyze the elements and valence states in B-nZVI. The research and test conditions were: the excitation source was Aika X-ray, the whole spectrum passing energy was 100 eV, and the step size was 1 eV.

## 3. Results and discussion

### 3.1. Characterization of composite materials

#### 3.1.1. Surface morphology analysis

Fig. 1a shows the scanning electron microscopy (SEM) diagram of nZVI, which produces self-agglomerations and is oxidized to oxides. Fig. 1b shows the bentonite-supported nano zerovalent iron material (B-nZVI). After the bentonite-supported nano zerovalent iron, spherical nano zerovalent iron particles exist in the lamellar and on the surface of the bentonite, as well as the nano zerovalent iron particles formed in chain shape and supported on the bentonite surface. Nano zerovalent iron supported on bentonite can greatly reduce the agglomeration and improve the dispersion compared with the unsupported nZVI [22,23]. At the same time, the adsorption properties of the

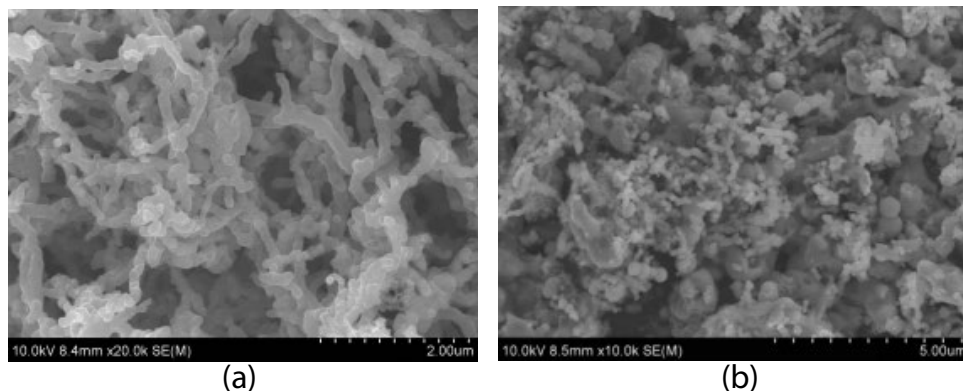


Fig. 1. SEM diagrams of different materials: (a) nZVI SEM and (b) B-nZVI.

bentonite were improved, and more active sites were added to increase the reactivity of the bentonite.

### 3.1.2. Surface functional group analysis

As can be seen from Fig. 2, in the spectra of bentonite and B-nZVI, the absorption peak at  $3,630\text{ cm}^{-1}$  is the vibration absorption peak of the hydroxyl group, the absorption peak at  $3,420$  and  $1,630\text{ cm}^{-1}$  is the bending vibration peak of H–O–H of water, and the absorption peak at  $2,850\text{ cm}^{-1}$  is the absorption peak of C–H.  $1,060\text{ cm}^{-1}$  is Si–O bending vibration peak,  $685\text{ cm}^{-1}$  absorption peak is Si–O deformation and bending vibration peak,  $520\text{ cm}^{-1}$  absorption peak is Al–Si–O bending vibration peak,  $460\text{ cm}^{-1}$  absorption peak is Si–O–Si bending vibration peak, The absorption peaks of  $1,060$  and  $2,850\text{ cm}^{-1}$  were weakened, which may be due to the destruction of Si–O bond and C–H bond during the preparation of B-nZVI. The peaks at  $540$  and  $470\text{ cm}^{-1}$  in the maps of nZVI and B-nZVI are The Fe–O stretching vibration peaks on  $\text{Fe}_2\text{O}_3$  and  $\text{Fe}_3\text{O}_4$  formed by oxidation. The results indicated that the nano zerovalent iron was successfully loaded on the surface of bentonite, retaining the characteristic functional groups of the original bentonite, and the nano zerovalent iron was oxidized on the surface.

### 3.1.3. Crystal structure analysis

Fig. 3 shows the X-ray diffraction (XRD) patterns of different materials. The characteristic  $\text{Fe}^0$  peak appears in B-nZVI at  $2\theta = 42^\circ\text{--}44^\circ$ . But the diffraction peak is relatively broad and diffuse compared with nZVI, while the diffraction peak of nanometer zerovalent iron has high intensity and sharp [24,25]. This indicates that the nano zerovalent iron adheres to the surface of bentonite or enters the pores inside it. But the amount of nano zerovalent iron is much smaller than that of nano zerovalent iron alone. The small peaks at about  $2\theta = 62^\circ$  are characteristic peaks of  $\text{Fe}_2\text{O}_3$  and  $\text{Fe}_3\text{O}_4$ .

### 3.1.4. X-ray photoelectron spectroscopy analysis

The X-ray photoelectron (XPS) spectrum of B-nZVI material is shown in Fig. 4. Fig. 4a is the full spectrum scan of the material, and Al, Si, K, O, Fe, Na and other characteristic peaks can be seen, indicating that the surface of the material is mainly composed of these elements. Fig. 4b shows the diagram of  $\text{Fe}2p$  XPS, with two significant peaks appearing at  $711$  and  $725\text{ eV}$ , respectively, which are mainly the oxides of divalent iron and trivalent iron [26]. This is due to the oxidation of zerovalent iron in the air of the prepared B-nZVI.

## 3.2. Influencing factors

### 3.2.1. Effect of different materials on removal of Cr(VI)

To compare the removal effect of three materials (B-nZVI, nZVI, and bentonite) on Cr(VI), the dosage of each material was  $1\text{ g/L}$ , and the mixture reaction was carried out with  $15\text{ mg/L}$  Cr(VI) solution in a constant temperature oscillator at  $35^\circ\text{C}$ , and the residual Cr(VI) concentration was measured after different time intervals.

According to Fig. 5, removal rates of Cr(VI) after the reaction of B-nZVI, nZVI, and bentonite with Cr(VI) solution for 1 h are 87%, 65% and 20%, respectively. It can be seen that B-nZVI has the best removal effect on Cr(VI). The removal effect of Cr(VI) by bentonite was the worst. This is because Cr(VI) mainly exists in the form of anion in aqueous solution, and the surface of bentonite is also electronegative, so it is difficult for Cr(VI) to be directly adsorbed on the surface of bentonite. The removal rate of Cr(VI) by nZVI is significantly lower than that of B-nZVI, mainly because the introduction of bentonite increases the dispersion and specific surface area of nanometer zerovalent iron so that nanometer zerovalent iron can obtain greater reactivity.

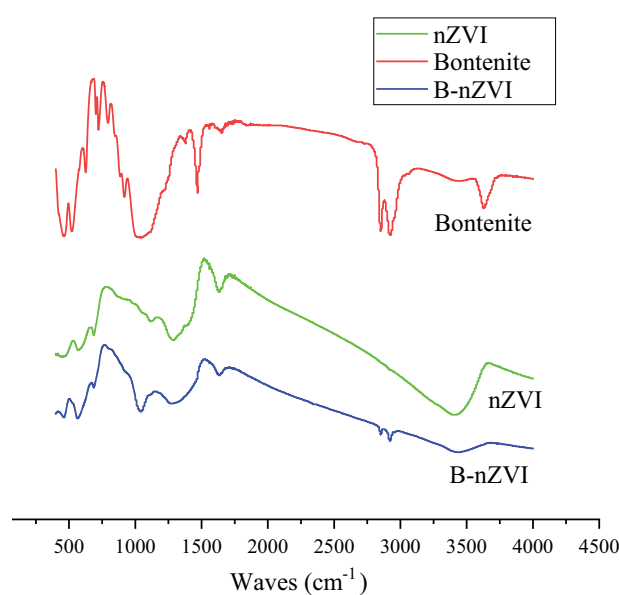


Fig. 2. Infrared absorption spectra of each material.

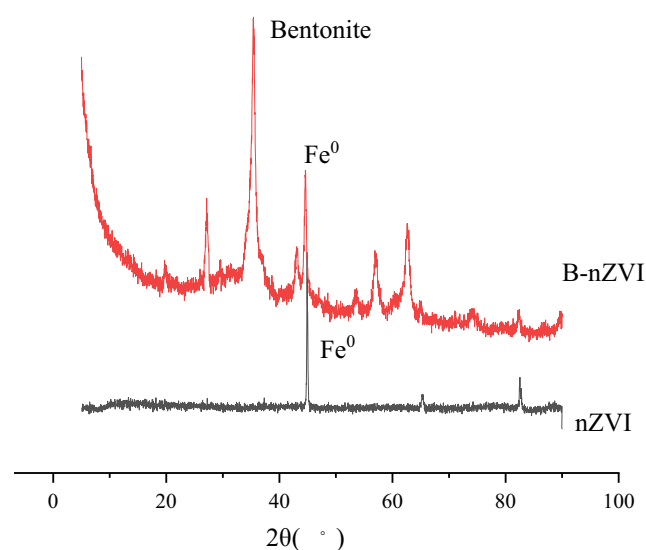


Fig. 3. XRD spectra of different materials.

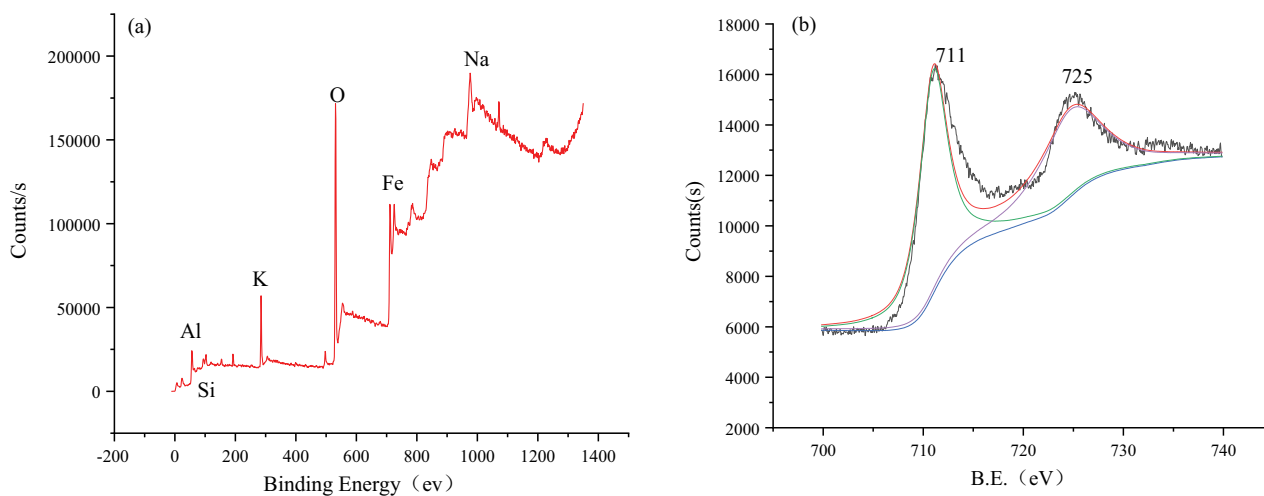


Fig. 4. XPS spectrum of B-nZVI: (a) full spectrum of B-nZVI and (b) Fe2p peak spectra.

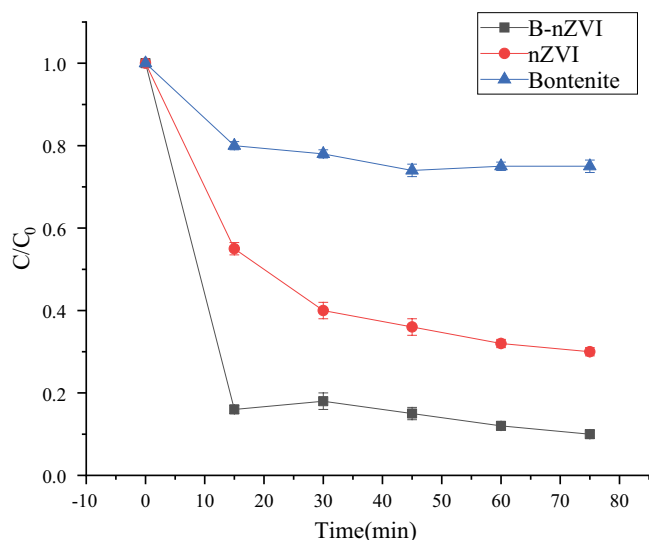


Fig. 5. Comparison of Cr(VI) removal performance of different materials.

### 3.2.2. Effect of pH value on removal of Cr(VI) by B-nZVI

The initial concentration of chromium was 15 mg/L, the dosage of B-nZVI was 1 g/L, and the effect of solution pH on the removal of chromium was compared at 35°C. As shown in Fig. 6, when the pH is 3, 4, 5, 7, and 9, the removal rate of B-nZVI on Cr(VI) gradually increases with the decrease of pH. When the pH is 9, the removal rate is only 45.6%; when the pH is 3, the removal rate can reach 96.9%; however, when the pH is 2. The results indicated that the optimal pH value was 3, Cr(VI) removal in the reaction was significantly inhibited under alkaline conditions, this is because acidic conditions can promote the corrosion of Fe in B-nZVI, remove the passivation film on the Fe surface, and thus improve the reaction efficiency. Under alkaline conditions, the formation of the hydroxide passivation layer will be promoted, and the reaction will be hindered [27]. The reduction of Cr(VI) by B-nZVI can be divided into direct and indirect effects. The immediate

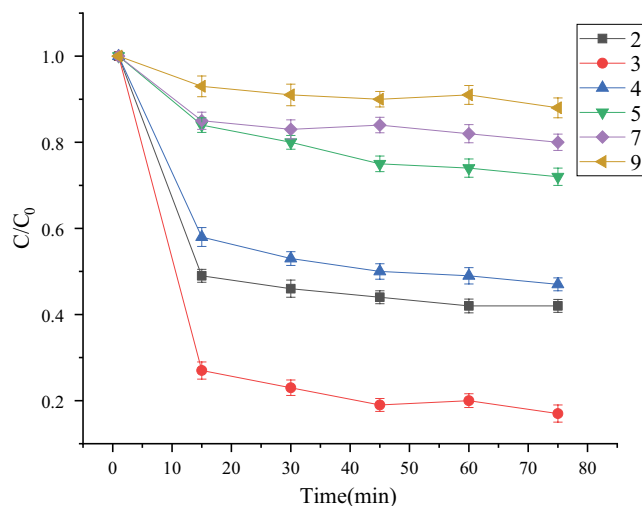


Fig. 6. Effect of pH on Cr(VI) removal by B-nZVI.

effect is the reduction of Cr(VI) by nZVI itself. Indirect action is the reduction of Cr(VI) by H<sub>2</sub> or H and Fe<sup>2+</sup> produced by oxidation and corrosion of nZVI in the water body.

### 3.2.3. Effect of temperature on Cr(VI) removal performance of B-nZVI

Under the conditions of pH 3, chromium concentration 15 mg/L, B-nZVI dosage 1 g/L, comparative temperature 20°C, 30°C, 35°C, 40°C, the adsorption effect of B-nZVI on Cr(VI) in the solution. The results are shown in Fig. 7. With the increase of temperature, the removal rate of Cr(VI) also increases, and the adsorption rate is 68%, 85%, 96%, and 98.9%, respectively. It is indicated that removing Cr(VI) from water by B-nZVI is an endothermic reaction, and the increase of reaction temperature is beneficial to the adsorption reaction. As the temperature increases, the molecular thermal motion is accelerated, and the reaction rate and adsorption rate of B-nZVI to Cr(VI) are improved.

In addition, the increase of temperature reduces the activation energy required for the reaction, which can accelerate the adsorption of B-nZVI and Cr(VI).

3.2.4. Effect of B-nZVI dosage on removal of Cr(VI)

When the pH is 3, the concentration of Cr(VI) is 15 mg/L, and the temperature is 35°C. The effects of different dosages of B-nZVI on the adsorption of Cr(VI) are compared, as shown in Fig. 8. With the increase of B-nZVI dosage, the removal rate of Cr(VI) also increased, and the removal rates were 45%, 78%, 97.6%, and 99.2%, respectively. When the material dosage increases from 1 to 1.2 g/L, the adsorption rate of chromium does not increase much because the adsorption sites of a certain amount of B-nZVI are limited [28]. In a particular concentration of Cr(VI) solution, with the increase of B-nZVI dosage, the number of adsorption sites available for Cr(VI) to contact additions. When the dosage

of adsorbent increases to a particular value, the adsorption effect will not be significantly improved by increasing the amount of adsorbent [29]. The optimal dosage of B-nZVI can remove chromium ions from the solution and avoid waste and economic loss. Therefore, when the concentration of Cr(VI) is 15 mg/L, the dosage of B-nZVI is 1 g/L, which can be regarded as the best adsorption dose.

3.2.5. Effect of initial concentration on removal of Cr(VI) by B-nZVI

When the dosage of B-nZVI is 1 g/L, the temperature is 35°C, the pH is 3, and the initial concentration of Cr(VI) is adjusted to 5, 10, 15, 20 and 30 mg/L, the removal effect of B-nZVI on Cr(VI) is shown in Fig. 9. Cr(VI) was rapidly adsorbed and degraded by B-nZVI 15 min before the reaction, and then the removal rate changed slowly. The initial Cr(VI) concentration has a great influence on the removal rate. The lower the initial Cr(VI) concentration

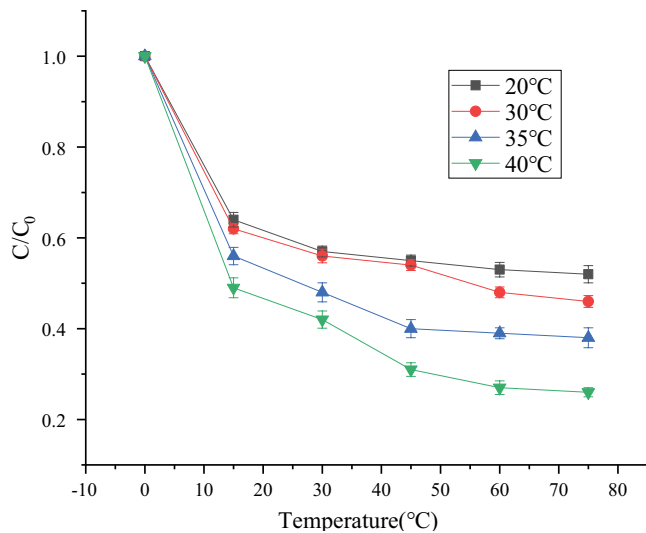


Fig. 7. Effect of temperature on Cr(VI) removal by B-nZVI.

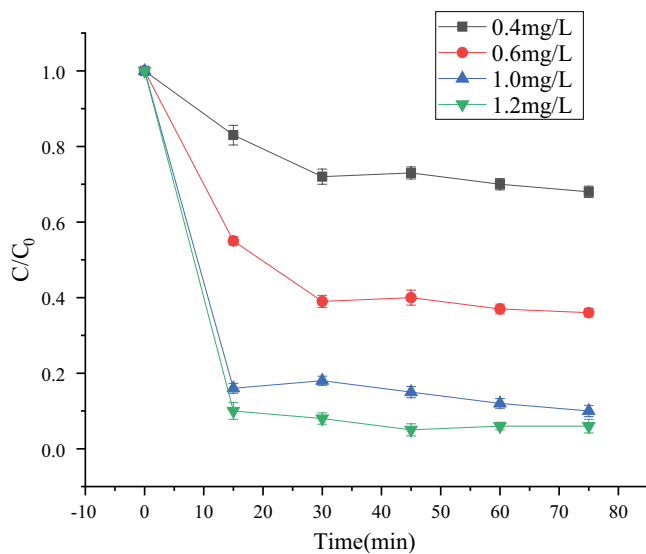


Fig. 8. Effect of dosage on Cr(VI) removal by B-nZVI.

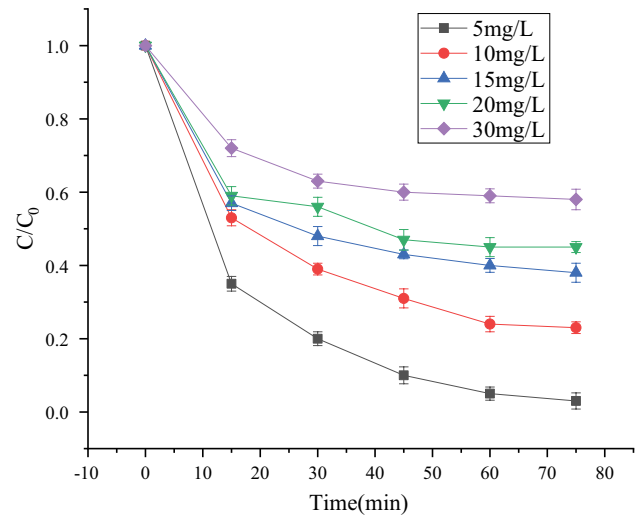


Fig. 9. Effect of initial concentration of Cr(VI) on removal of Cr(VI) by B-nZVI.

is, the higher the removal rate is. When the initial concentration of Cr(VI) is 5 mg/L, the adsorption rate of B-nZVI for Cr(VI) can reach 99.8% at 75 min. With the increase of the initial concentration of Cr(VI), the removal rate of Cr(VI) decreases gradually. This is because when the dosage of B-nZVI is fixed, the contact between Cr(VI) and B-nZVI decreases with the increase of the initial concentration, and the reaction sites and adsorption sites also decrease, which affects the removal effect of Cr(VI).

### 3.2.6. Effect of coexisting ions

In order to explore the effect of coexisting ions on the removal of Cr(VI) by B-nZVI, five common ions in water, such as  $\text{Ca}^{2+}$ ,  $\text{K}^+$ ,  $\text{Mg}^{2+}$ ,  $\text{SO}_4^{2-}$  and  $\text{CO}_3^{2-}$ , were selected as coexisting ions, and the ion concentration was 100 mg/L, and the dosage of B-nZVI was 1 g/L. The initial concentration of Cr(VI) was 15 mg/L, and the reaction time was 60 min.

The presence of a cation affects the presence of the reaction process, but the anion should be larger than the anion.  $\text{K}^+$  has the least effect, followed by  $\text{Ca}^{2+}$  and  $\text{Mg}^{2+}$ , and  $\text{SO}_4^{2-}$  and  $\text{CO}_3^{2-}$  have the most effect.  $\text{Ca}^{2+}$  and  $\text{Mg}^{2+}$  occupy the adsorption sites on the surface of the composite. In addition, a large amount of  $\text{H}^+$  is consumed during the reaction between nZVI and Cr(VI). With the progress of the reaction, the pH of the system gradually rises, forming  $\text{Fe}(\text{OH})_3$  or  $\text{Cr}(\text{OH})_3$  or iron-chromium co-precipitate on the surface of nZVI, which impedes the external transfer of electrons produced by nZVI. The removal efficiency of Cr(VI) decreased. The hydrolysis of  $\text{CO}_3^{2-}$  in water produces a large amount of  $\text{OH}^-$ , which leads to the increase of solution pH, and the removal rate of Cr(VI) by B-nZVI will be reduced under high pH conditions. In addition,  $\text{CO}_3^{2-}$  interacts with Fe(II) produced by nZVI corrosion to form insoluble substances that hinder the reaction.  $\text{SO}_4^{2-}$  will compete with Cr(VI) for reaction sites on the nZVI surface, resulting in inhibition of the reaction.

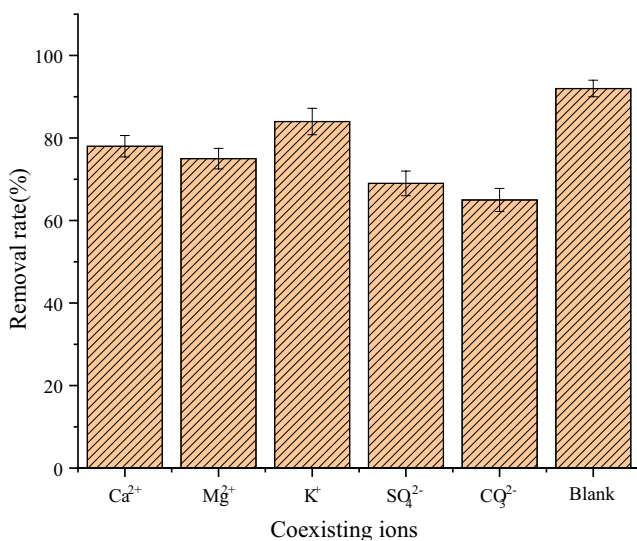


Fig. 10. Effect of B-nZVI on Cr(VI) removal in the presence of different ions.

### 3.2.7. Material reuse

Fig. 11 shows the effect of B-nZVI and nZVI reuse times on Cr(VI) removal.

With the increase of use times, the removal rate of Cr(VI) from nZVI decreased significantly. At the fifth utilization, the removal rate had dropped to 18.60%. In contrast, the performance of B-nZVI is better than that of nZVI, the removal rate dropped to 33.20%, because it is loaded with bentonite. The loading of bentonite can effectively prevent the agglomeration of nZVI and provide more active sites for the reduction of Cr(VI). It can be inferred from the experimental phenomenon that the reaction between nanometer zerovalent iron and Cr(VI) is irreversible. The fact that zerovalent iron is consumed and the hydroxide produced by the reaction is attached to the iron suggests that the reduction of the reaction site is an important reason for the reduced efficiency. By fixing nanometer zerovalent iron on bentonite, it can not only act as the dispersant but also adsorb Cr(VI) on its surface so that nZVI can easily react with Cr(VI).

### 3.3. Response kinetics analysis of Cr(VI) removal by B-nZVI

The removal of Cr(VI) by B-nZVI is a heterogeneous reaction process occurring on the surface of the material. The pseudo-first-order kinetic equation can better fit the reaction process.

The pseudo-first-order kinetic model assumes that the adsorption rate of the adsorbent is directly proportional to the concentration of the adsorbent.

$$\ln\left(\frac{C}{C_0}\right) = -k_{\text{obs}} t \quad (1)$$

where  $k_{\text{obs}}$  is the apparent rate constant ( $\text{min}^{-1}$ );  $C$  and  $C_0$  are respectively the concentration of Cr at the initial reaction (mg/L) and the concentration of Cr at the time  $t$  (mg/L).

When the pH of the solution is 3, the  $k_{\text{obs}}$  of the reaction reaches the maximum, the pH increases from 3 to 9, and the

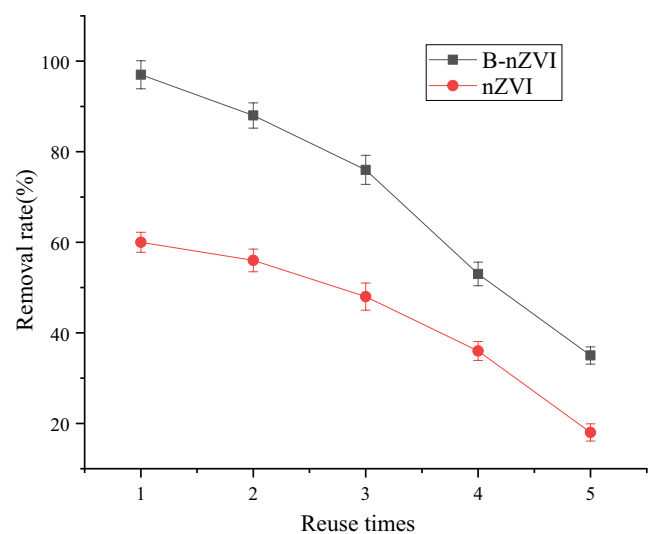


Fig. 11. Effect of reuse times on Cr(VI) removal rate.

$k_{obs}$  decrease from 0.0071 to 0.0009 min<sup>-1</sup>, and the reaction rate gradually decreases. With the increase of temperature,  $k_{obs}$  increase from 0.005 to 0.0114 min<sup>-1</sup>, which provides part of the activation energy required for the reaction between B-nZVI and Cr(VI). The higher the temperature, the less the activation energy required for the reaction and the faster the reaction rate. The smaller the initial concentration of Cr, the larger the  $k_{obs}$ . The initial concentration of Cr increases from 5 to 30 mg/L, and the corresponding  $k_{obs}$  are 0.0185, 0.0144, 0.0066, 0.0051 and 0.0036 min<sup>-1</sup>. With the increase of B-nZVI dosage,  $k_{obs}$  increased from 0.0029 to 0.0116. It shows that increasing the dosage of B-nZVI makes Cr contact with more nZVI, and the reduction reaction occurs, and the reaction rate increases.

3.4. Mechanism analysis of Cr(VI) removal by B-nZVI

Bentonite has a large specific surface area and has a certain adsorption capacity. After loading nZVI, it can

disperse nanometer zerovalent iron particles and reduce their agglomeration. Under acidic conditions, Cr(VI) was first adsorbed on the surface of B-nZVI, and then reduced to Cr(III) by nanometer zerovalent iron supported on bentonite. The nanometer zerovalent iron was generated from Fe<sup>0</sup> to Fe(II), and Fe(II) could continue to reduce Cr(VI) to Cr(III), and Fe(II) was converted to Fe(III). The resulting Cr(III) and Fe(III) cover the surface of B-nZVI on Fe<sup>0</sup>, forming ferric chromium co-precipitate and a passivation layer, which hinders the electron transfer from Fe<sup>0</sup> to Cr(VI) and reduce the rate of the reduction reaction. The main reaction process is shown in the following formula.

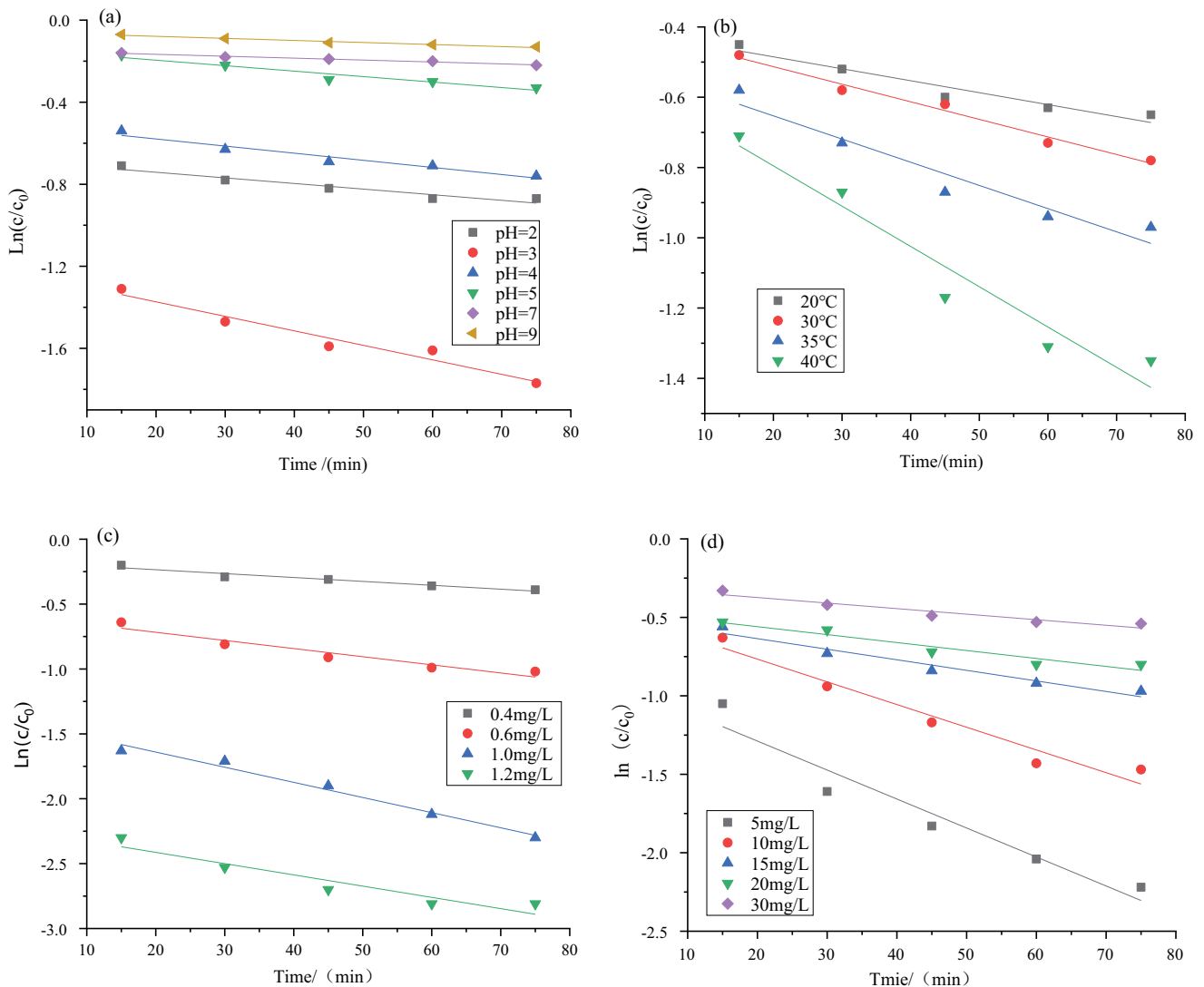
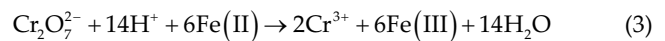
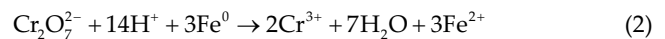
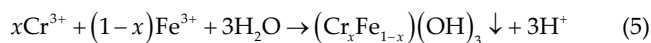
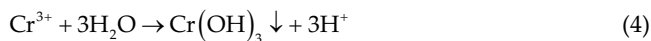


Fig. 12. Relationship curve between  $\ln(C/C_0)$  and  $t$  at different: (a) initial pH, (b) temperatures, (c) B-nZVI dosage, and (d) initial Cr concentrations.



#### 4. Conclusion

- The material characterization results showed that after the bentonite was loaded with nano-valent iron, there were spherical nanovalent iron particles on the lamina and surface of bentonite, which reduced the agglomeration phenomenon of nZVI and improved its dispersion; The original characteristic functional groups of bentonite are retained.
- The pH value and initial concentration of Cr(VI) had a great influence on the removal of Cr(VI). The removal effect of Cr(VI) under acidic conditions was better than that under alkaline conditions. The lower the initial concentration of Cr(VI), the better the removal effect. With the decrease of temperature and B-nZVI dosage, the removal rate of Cr(VI) decreases, and the influence of coexisting cation is less than that of the coexisting anion.
- The reaction mechanism of B-nZVI removal of Cr(VI) is as follows: first, B-nZVI adsorbs Cr(VI) to its surface, then  $\text{Fe}^0$  reduces it to Cr(III), and then it is removed by forming chromium precipitate or ferric chromium co-precipitate.

#### Acknowledgements

The study was financially supported by the Jiangsu construction system science and technology project(2019ZD034), supported by the Key Laboratory of Jiangxi Province for Persistent Pollutants Control and Resources Recycle (ES201980193), supported by Natural Science Foundation of colleges and universities of Jiangsu Provincial Department of Education (21KJA610006).

#### References

- [1] S. Mishra, R.N. Bharagava, N. More, A. Yadav, S. Zainith, S. Mani, P. Chowdhary, Heavy Metal Contamination: An Alarming Threat to Environment and Human Health, Dr. Ranbir Chander Sobti, Prof. Naveen Kumar Arora, Dr. Richa Kothari, Eds. Environmental Biotechnology: For Sustainable Future, Springer, Singapore, 2019, pp. 103–125.
- [2] P. Chowdhary, R.N. Bharagava, S. Mishra, N. Khan, Role of Industries in Water Scarcity and Its Adverse Effects on Environment and Human Health, V. Shukla, N. Kumar, Eds., Environmental Concerns and Sustainable Development, Springer, Singapore, 2020, pp. 235–256.
- [3] B. He, Z.J. Yun, J.B. Shi, G.B. Jiang, Research progress of heavy metal pollution in China: sources, analytical methods, status, and toxicity, Chin. Sci. Bull., 58 (2013) 134–140.
- [4] B. Dhal, H.N. Thatoi, N.N. Das, B.D. Pandey, Chemical and microbial remediation of hexavalent chromium from contaminated soil and mining/metallurgical solid waste: a review, J. Hazard. Mater., 250 (2013) 272–291.
- [5] H. Ma, J. Yang, X. Gao, Z. Liu, X. Liu, Z. Xu, Removal of chromium (VI) from water by porous carbon derived from corn straw: influencing factors, regeneration and mechanism, J. Hazard. Mater., 369 (2019) 550–560.
- [6] Y. Yi, X. Wang, J. Ma, P. Ning, An efficient *Egeria najas*-derived biochar supported nZVI composite for Cr(VI) removal: characterization and mechanism investigation based on visual MINTEQ model, Environ. Res., 189 (2020) 109912, doi: 10.1016/j.envres.2020.109912.
- [7] F. Zhu, T. Liu, Z. Zhang, W. Liang, Remediation of hexavalent chromium in column by green synthesized nanoscale zerovalent iron/nickel: factors, migration model and numerical simulation, Ecotoxicol. Environ. Saf., 207 (2021) 111572, doi: 10.1016/j.ecoenv.2020.111572.
- [8] M. Al Osman, F. Yang, I.Y. Massey, Exposure routes and health effects of heavy metals on children, Biometals, 32 (2019) 563–573.
- [9] N.M. Izzudin, A.A. Jalil, F.F.A. Aziz, M.S. Azami, M.W. Ali, N.S. Hassan, A.F.A. Rahman, A.A. Fauzi, D.V.N. Vo, Simultaneous remediation of hexavalent chromium and organic pollutants in wastewater using period 4 transition metal oxide-based photocatalysts: a review, Environ. Chem. Lett., 19 (2021) 4489–4517.
- [10] S. Mishra, R.N. Bharagava, Toxic and genotoxic effects of hexavalent chromium in environment and its bioremediation strategies, J. Environ. Sci. Health., Part C Environ. Carcinog. Ecotoxicol. Rev., 34 (2016) 1–32.
- [11] X. Deng, Y. Chen, J. Wen, Y. Xu, J. Zhu, Z. Bian, Polyaniline-TiO<sub>2</sub> composite photocatalysts for light-driven hexavalent chromium ions reduction, Sci. Bull., 65 (2020) 105–112.
- [12] Z. Rahman, V.P. Singh, Bioremediation of toxic heavy metals (THMs) contaminated sites: concepts, applications and challenges, Environ. Sci. Pollut. Res., 27 (2020) 27563–27581.
- [13] N. Ezzatahmedi, G.A. Ayoko, G.J. Millar, R. Speight, C. Yan, J. Li, S. Li, J. Zhu, Y. Xi, Clay-supported nanoscale zerovalent iron composite materials for the remediation of contaminated aqueous solutions: a review, Chem. Eng. J., 312 (2017) 336–350.
- [14] Y. Zhou, T. Wang, D. Zhi, B. Guo, Y. Zhou, J. Nie, A. Huang, Y. Yang, H. Huang, L. Luo, Applications of nanoscale zerovalent iron and its composites to the removal of antibiotics: a review, J. Mater. Sci., 54 (2019) 12171–12188.
- [15] H. Tang, J. Wang, S. Zhang, H. Pang, X. Wang, Z. Chen, M. Li, G. Song, M. Qiu, S. Yu, Recent advances in nanoscale zerovalent iron-based materials: characteristics, environmental remediation and challenges, J. Cleaner Prod., 319 (2021) 128641, doi: 10.1016/j.jclepro.2021.128641.
- [16] Tang, H. Wang, J. Zhang, S. Pang, H. Wang, X. & Chen, Z. Mechanisms of enhanced hexavalent chromium removal from groundwater by sodium carboxymethyl cellulose stabilized zerovalent iron nanoparticles. Journal of Environmental Management, 319(2021)276: 111245.
- [17] J. Li, M. Fan, M. Li, X. Liu, Cr(VI) removal from groundwater using double surfactant-modified nanoscale zerovalent iron (nZVI): effects of materials in different status, Sci. Total Environ., 717 (2020) 137112, doi: 10.1016/j.scitotenv.2020.137112.
- [18] Y. Dai, Y. Hu, B. Jiang, J. Zou, G. Tian, H. Fu, Carbothermal synthesis of ordered mesoporous carbon-supported nano zerovalent iron with enhanced stability and activity for hexavalent chromium reduction, J. Hazard. Mater., 309 (2016) 249–258.
- [19] B. Zhang, D. Wang, Preparation of biomass activated carbon supported nanoscale zerovalent iron (nZVI) and its application in decolorization of methyl orange from aqueous solution, Water, 11 (2019) 1671, doi: 10.3390/w11081671.
- [20] J. Ma, J. Zou, L. Li, C. Yao, T. Zhang, D. Li, Synthesis and characterization of Ag<sub>3</sub>PO<sub>4</sub> immobilized in bentonite for the sunlight-driven degradation of Orange II, Appl. Catal., B, 134–135 (2013) 1–6.
- [21] J.A. Alexander, M.A. Ahmad Zaini, A. Surajudeen, E.-N. Usman Aliyu, A.U. Omeiza, Surface modification of low-cost bentonite adsorbents—a review, Part. Sci. Technol., 37 (2019) 538–549.
- [22] E. Petala, K. Dimos, A. Douvalis, T. Bakas, J. Tucek, R. Zbořil, M.A. Karakassides, Nanoscale zerovalent iron supported on mesoporous silica: characterization and reactivity for Cr(VI)

- removal from aqueous solution, *J. Hazard. Mater.*, 261 (2013) 295–306.
- [23] G. Wei, J. Zhang, J. Luo, H. Xue, D. Huang, Z. Cheng, X. Jiang, Nanoscale zerovalent iron supported on biochar for the highly efficient removal of nitrobenzene, *Front. Environ. Sci. Eng.*, 13 (2019), doi: 10.1007/s11783-019-1142-3.
- [24] S.-H. Zhang, M.-F. Wu, T.-T. Tang, Q.-J. Xing, C.-Q. Peng, F. Li, H. Liu, X.-B. Luo, J.-P. Zou, X.-B. Min, J.-M. Luo, Mechanism investigation of anoxic Cr(VI) removal by nano zerovalent iron based on XPS analysis in time scale, *Chem. Eng. J.*, 335 (2018) 945–953.
- [25] Y. Hu, X. Peng, Z. Ai, F. Jia, L. Zhang, Liquid nitrogen activation of zerovalent iron and its enhanced Cr(VI) removal performance, *Environ. Sci. Technol.*, 53 (2019) 8333–8341.
- [26] Y. Li, M. Deng, X. Wang, Y. Wang, J. Li, S. Xia, J. Zhao, In-situ remediation of oxytetracycline and Cr(VI) co-contaminated soil and groundwater by using blast furnace slag-supported nanosized Fe<sup>0</sup>/FeS<sub>x</sub>, *Chem. Eng. J.*, 412 (2021) 128706, doi: 10.1016/j.cej.2021.128706.
- [27] U. Malayoglu, Removal of heavy metals by biopolymer (chitosan)/nanoclay composites, *Sep. Sci. Technol.*, 53 (2018) 2741–2749.
- [28] W. Wang, J. Wang, Y. Guo, C. Zhu, F. Pan, R. Wu, C. Wang, Removal of multiple nitrosamines from aqueous solution by nanoscale zerovalent iron supported on granular activated carbon: influencing factors and reaction mechanism, *Sci. Total Environ.*, 639 (2018) 934–943.
- [29] Z. Zhang, P. Gao, J. Cheng, G. Liu, X. Zhang, Y. Feng, Enhancing anaerobic digestion and methane production of tetracycline wastewater in EGSB reactor with GAC/nZVI mediator. *Water research*, 136(2018) 54–63.